Physics in Collision - Stanford, California, June 20-22, 2002

RELATIVISTIC HEAVY ION PHYSICS: RESULTS FROM AGS TO RHIC

Peter Steinberg
Brookhaven National Laboratory, Upton, New York, USA

ABSTRACT

High-energy collisions of heavy ions provide a means to study QCD in a regime of high parton density, and may provide insight into its phase structure. Results from the four experiments at RHIC (BRAHMS, PHENIX, PHOBOS and STAR) are presented, and placed in context with the lower energy data from the AGS and SPS accelerators. The focus is on the insights these measurements provide into the time history of the collision process. Taken together, the data point to the creation of a deconfined state of matter that forms quickly, expands rapidly and freezes out suddenly.

1 Introduction

The goal of high energy heavy ion physics is to study QCD in a regime of high temperature, high density, and large reaction volumes. The hope is to find conclusive evidence that QCD undergoes a phase transition at a critical temperature from a confined state, where quarks and gluons are bound in colorless hadron states, to a deconfined quark-gluon plasma (QGP), where quarks and gluons can explore volumes larger than the typical hadron radius ($R \sim 1$ fm). Lattice calculations, under a variety of assumptions (e.g. number of quark flavors or m_s), make the robust prediction that the degrees of freedom available to the system rise rapidly as it is heated through the critical temperature $T_c \sim 150 - 200$ MeV [1], as shown in Fig. 1. This corresponds to an energy density of order $\epsilon_c \sim 1 - 2$ GeV/fm^3. There is great interest within the theoretical community whether these lattice predictions will be confirmed in experiments and, more generally, whether high temperature QCD can be used to make quantitative predictions.

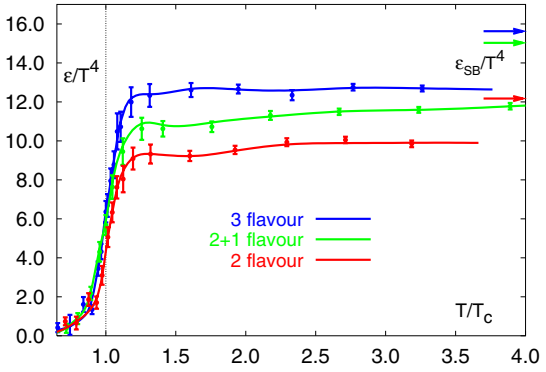

Figure 1: Lattice predictions for the energy density as a function of T/T_c.

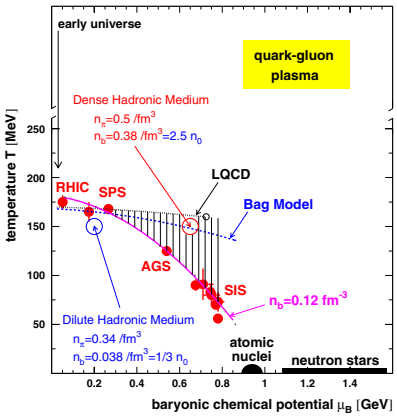

Figure 2: Theoretical expectations for the QCD phase diagram.

While the theoretical questions are compelling in themselves, the experimental challenges of measuring the properties of heavy ion collisions in the laboratory imply a related set of questions that should be addressed before definitive theoretical conclusions can be made. The overarching problem is whether it is possible to discern the various stages in the time evolution of the system, which evolves from the initial collisions to the final state hadrons in times on the order of 10's of fm/c. To discover a QGP formed in the early stages of the collision, there must be

observables which maintain information about its properties throughout the expansion and cooling of the system and the final hadronization stage which forms many of the particles that register in the experimental apparatus.

While measurables which address the early times directly (e.g. lepton and photon observables) are becoming available, the emphasis here will be on hadronic observables. The claim in this proceedings is that the evidence collected so far points to a picture of the collision dynamics which is consistent with the formation of a deconfined state that forms quickly, expands rapidly, and freezes out suddenly. There are also interesting comparisons with charged particle production in e^+e^- collisions that provides some connections with perturbative QCD phenomenology.

2 Colliders & Experiments

High energy beams of heavy nuclei have been available at the Brookhaven AGS (Au+Au at the CMS energies per NN collision from $\sqrt{s_{NN}} = 2.5 - 4.3$ GeV). and the CERN SPS (Pb+Pb collisions from $\sqrt{s_{NN}} = 8 - 17.3$ GeV). Since then, a new collider, RHIC, has begun colliding nuclei at higher energies (up to $\sqrt{s_{NN}} = 200$ GeV) with substantial luminosities (of up to $10^{26}\text{sec}^{-1}\text{cm}^2$). The results shown here focus primarily on RHIC data from Au+Au collisions over a range of energies ($\sqrt{s_{NN}}$ = 19.6, 56, 130 and 200 GeV). Most of the results are from the 130 GeV run, where the available luminosity limited the p_T reach of many observables. However, early results from the 200 GeV data are shown here, and some preliminary results shown at the recent Quark Matter conference are also mentioned [2].

There are four RHIC experiments, which can be classified into two groups: the "large" experiments, PHENIX and STAR, which are large-volume and large-acceptance general-purpose detectors, and the "small" experiments, BRAHMS and PHOBOS, which are have more limited acceptance but cover aspects of the collisions not addressed by the other experiments. STAR has a large TPC with coverage for charged hadrons in $|\eta| < 1$ and particle identification via dE/dx up to $p_T \sim 1$ GeV. PHENIX has more limited hadron coverage ($|\eta| < .35$) but a higher data rate, extensive particle identification for hadrons, photons, and electrons, and forward muon arms. PHOBOS has a small-acceptance silicon spectrometer near $y \sim 1$ and 4π acceptance for multiplicity measurements. BRAHMS has two movable multi-particle spectrometers, one at midrapidity, and one covering rapidities out to $y \sim 4$, offering a look at identified particle spectra in regions not covered by any of the other RHIC experiments. The four RHIC experiments complement each other in that they study many different aspects of heavy ion collisions, but all have hadron coverage

near mid-rapidity, which allows detailed cross-checks between the experiments.

3 Initial Conditions

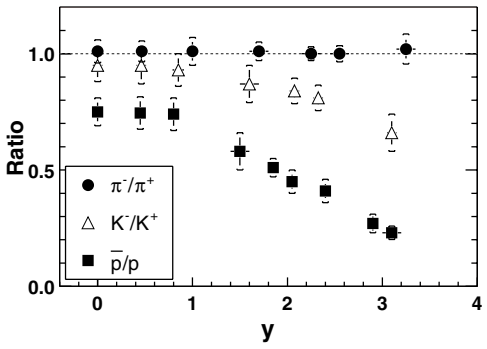

Figure 3: Ratios of particles to antiparticles vs. rapidity, from the BRAHMS experiment.

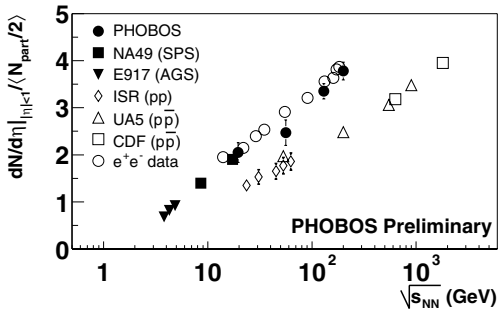

Figure 4: Charged particle density at midrapidity, for e^+e^-, pp and Au+Au collisions.

The initial conditions of heavy ion collisions are determined primarily by the beam energy and the nuclear geometry. The impact parameter between the nuclei controls the overlap area of the contracted nuclei and thus the number of nucleons which participate via inelastic processes (N_{part}) and the number of binary collisions ($N_{coll} \propto N_{part}^{\frac{4}{3}}$) The beam energy determines the initial state parton density, which is dominated by gluons at low-x, the available range in rapidity ($\Delta y = 2\ln(\sqrt{s}/m_p)$), and the total nucleon-nucleon cross section. The combination of these factors contribute to the amount of energy deposited by the incoming baryons in each nucleus as they lose energy while penetrating the other nucleus – a phenomenon called "proton stopping" This is typically measured by the net rapidity distribution of protons minus anti-protons. Recent results from BRAHMS [3] show that while the ratio of protons to anti-protons is about 0.75 at mid-rapidity, it falls rapidly by $y = 3$, consistent with a rapid increase in the net proton density, which is expected to peak at a rapidity 2.5 units from $y_{\rm beam}$[4]. These measurements will be critical for understanding the very early collision stage.

All of the RHIC experiments perform measurement at midrapidity, where hard processes are expected to contribute substantially to particle production. The energy density achieved in the collisions can be estimated either by measuring the transverse energy and using the Bjorken formula $\epsilon = (dE_T/dy)/\pi R^2 \tau_o$, with R the nuclear radius and τ_o the "formation time" of the system. PHENIX has measured

the transverse energy density at midrapidity in 130 GeV Au+Au collisions and extracted an energy density $\epsilon = 4.6$ GeV/fm^3 [5] assuming at typical value for $\tau_o \sim 1$ fm/c. This is already well above lattice expectations for a QGP phase transition. They have also found the ratio E_T/N_{ch} to be constant for all N_{ch}. Thus, one can use the ratio of midrapidity charged particle production at 130 and 200 GeV ($R = 1.14 \pm .05$), shown in Fig. 4 as the particle production per participant pair [6], to infer an energy density of about $\epsilon = 5.3$ GeV/fm^3 at the highest RHIC energies.

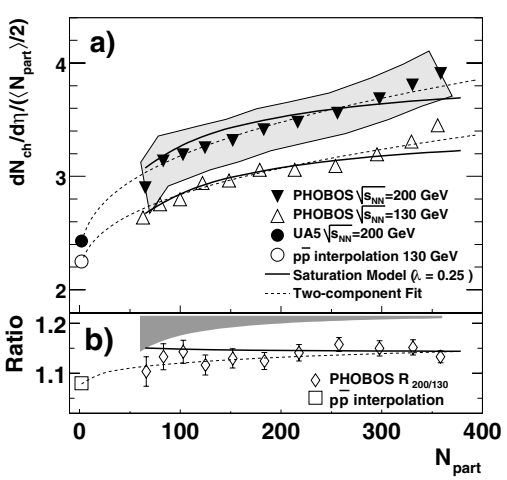

Figure 5: Centrality dependence of $dN_{ch}/d\eta/\langle N_{part}/2\rangle$ compared with two-component and saturation models.

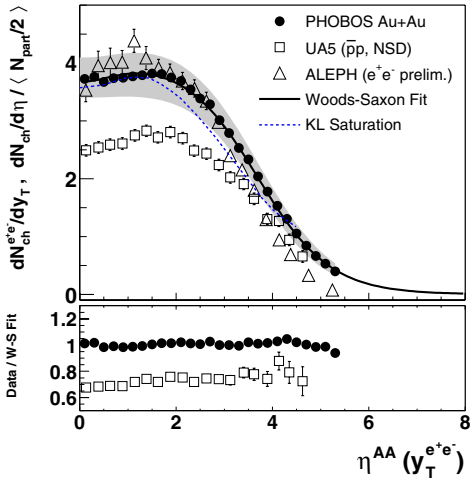

Figure 6: Pseudorapidity distributions of Au+Au, $\overline{p}p$ and e^+e^- at $\sqrt{s}$=200 GeV. The parton saturation prediction of Ref. [9] is also shown.

The centrality dependence of charged particle production, $dN_{ch}/d\eta/\langle N_{part}/2\rangle$, offers a means to study the evolution between pp collisions and central Au+Au. Two types of predictions [7] have proven effective in describing the midrapidity data [6] shown in Fig. 5. The "two-component" model postulates that the total particle production stems from a linear combination of soft processes that scale with the number of participants, and hard processes that scale with the number of binary collisions. Thus, $dN_{ch}/d\eta = n_{pp}((1 - X(s))N_{part}/2 + X(s)N_{coll})$, where n_{pp} is the measured multiplicity in pp collisions, and $X(s)$ is the energy-dependent fraction of hard processes in pp collisions. (approximately 0.1 at RHIC). It is also expected that the energy released in the form of low-x gluons should create a parton density so high that the partons below a "saturation scale" Q_s (i.e. of larger transverse size) recombine in order not to exceed a maximum value of order $1/\alpha_s(s)$ [8]. In this picture, particle production is determined mainly by Q_s, which itself depends on the

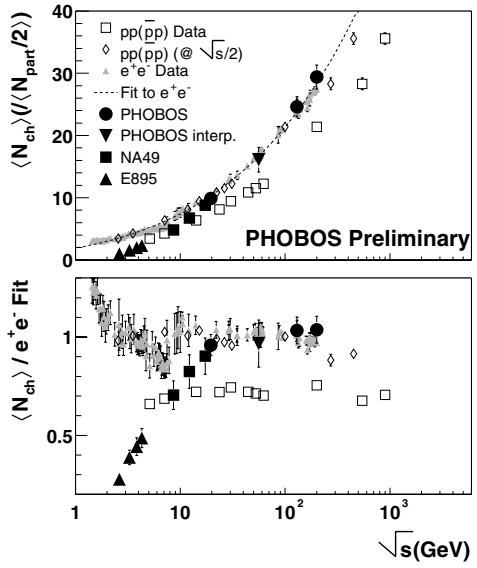

Figure 7: Total charged particle production for a variety of strongly-interacting systems. Comparison with a fit to the e^+e^- data is shown.

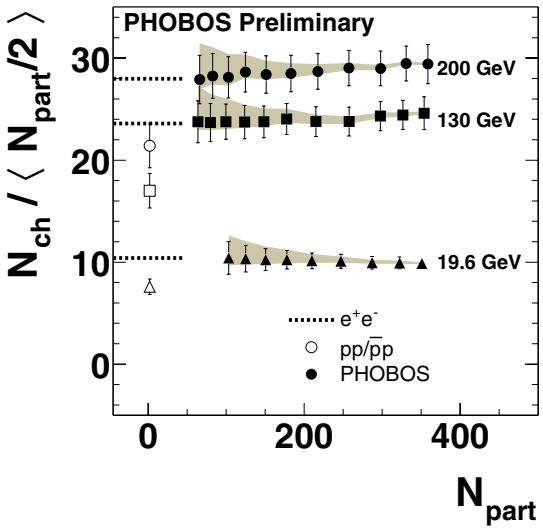

Figure 8: Total multiplicity per participant pair for Au+Au collisions at $\sqrt{s_{NN}} = 19.6, 130$, and 200 GeV.

transverse density of partons (i.e. $Q_s^2 \propto A^{1/3}$), $dN_{ch}/d\eta/\langle N_{part}/2\rangle = 1/\alpha_s(Q_s^2)$. As shown in Fig. 5, both of these models offer an efficient description of the experimental data from all of the RHIC experiments. Saturation models are also able to offer a reasonable quantitative description of the full rapidity distribution, an example of which by Kharzeev and Levin [9] is shown as a dotted line in Fig. 6.

The success of the saturation models in capturing basic features of particle production has a fascinating consequence. While most expectations of the "formation time" τ_0 used in energy density estimates are around 1 fm/c, saturation models predict the formation time of the initial gluon state to be $\tau_s \sim \hbar/Q_s \sim .2$ fm/c, which gives $\epsilon \sim 18$ GeV/fm^3 when plugged into the Bjorken formula for the 130 GeV data. While neither estimate (5 GeV/fm^3 or 18 GeV/fm^3) should be taken too seriously at this point, these estimates show that both naive and more sophisticated estimates arrive at values well above the lattice expectations for QGP formation.

4 Universal Features of Particle Production

We can gain insight into the relationship between Au+Au collisions and elementary nucleon-nucleon interactions by comparisons with e^+e^- annihilations to hadrons. It has long been noted that the charged multiplicities in pp and e^+e^- collisions are

similar if the energy taken away by the "leading baryons" is subtracted from $\sqrt{s}$ and then compared to e^+e^- collisions at this $\sqrt{s_{\rm eff}}$, suggesting a universal fragmentation mechanism [10]. With new data from RHIC and LEP2, PHOBOS finds that Au+Au (divided by the number of participant pairs $\langle N_{part}/2\rangle$) and e^+e^- collisions have similar pseudorapidity densities over a large range (see Fig. 6) and thus a similar total multiplicity [11]. Comparisons of the total multiplicity per participant pair $\langle N_{ch}\rangle/\langle N_{part}/2\rangle$ over a large range of CMS energies is shown in Fig. 7 and compared to e^+e^- and $pp/\overline{p}p$ data. It is easiest to compare these data sets by dividing all of the values vs. $\sqrt{s}$ by a function that describes the e^+e^- data [12]. It is seen that the Au+Au and e^+e^- data converge for $\sqrt{s} > 20$ GeV, while the pp data also follows the same trend if the effective energy $\sqrt{s_{\rm eff}} = \sqrt{s}/2$ is used.

The total multiplicity produced per participant pair in Au+Au collisions has also been measured by PHOBOS. It is shown in Fig. 8 to be constant over the range of centralities measured ($N_{part} > 65$) for all three energies [11]. This is reminiscent of "wounded-nucleon" scaling [13] but in all three cases the multiplicity is about 30-40% higher than pp at comparable energy, and comparable to e^+e^-. This adds an interesting perspective to the use of minijet and saturation approaches in describing the multiplicity at $\eta = 0$, as discussed in the previous section.

This similarity in bulk particle production between Au+Au and e^+e^- data for $\sqrt{s} > 20$ GeV suggests that Au+Au are more efficient than NN interactions in transferring the incoming energy into particle production. This might simply indicate that the multiple collisions suffered per participant substantially reduce the leading particle effect. The drop below 20 GeV may be explained by the presence of a large baryon density in the final state [14]. While it is obvious that Au+Au collisions do not start with the same initial scale as e^+e^-, which is reflected in the much harder p_T distributions in e^+e^- above 2 GeV, it appears that the available energy, rather than the initial hard scale, has the stronger effect on the bulk particle production. This may be another manifestation of the universality of low-x physics in strongly-interacting systems at high energy (which is discussed in the HERA context in Ref. [15]). The physics behind this may need to be addressed before claims to particular behavior for particle yields in heavy ions can be made in other contexts.

5 Dynamics of the Parton Cascade

If the energy density is indeed as large, and forms as early, as the success of the saturation descriptions seem to imply, then we might expect the density of scatterings to

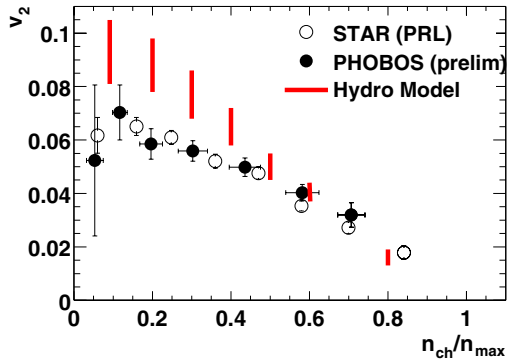

Figure 9: Data from STAR and PHOBOS on elliptic flow vs. collision centrality compared to hydrodynamic predictions.

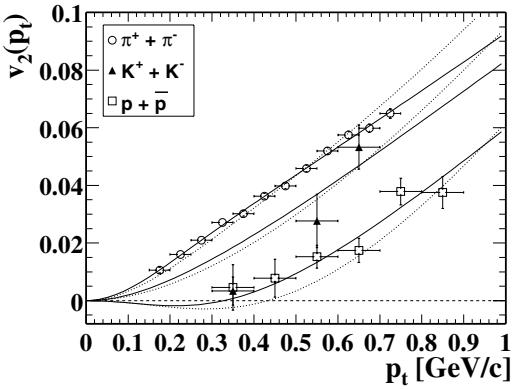

Figure 10: STAR data on v_2 vs. p_T for different particles species, also compared with hydro calculations.

lead to an early thermalization and possibly the development of hydrodynamic behavior as the system evolves [16]. This expectation is borne out by measurements of the event-by-event azimuthal distributions, which are found to have a slightly elliptical shape at all energies from AGS to RHIC. The maximum value of v_2, the second Fourier component of the azimuthal distribution, $dN/d\phi \propto 1 + 2v_2 \times \cos(2(\phi - \Psi_R))$ with Ψ_R the angle of the event reaction plane, has been found to increase with increasing beam energy. This is contrary to what one would expect if the dynamics were purely hadronic, since late stage rescattering would wash out any initial state anisotropy. Thus, the non-zero v_2 has been interpreted as stemming from hydrodynamic pressure gradients in the initial state, implying partonic thermalization, which is an essential prerequisite to QGP formation.

The results from STAR and PHOBOS [17, 18] are shown in Fig. 9 and compared with predictions from a range of hydro models (shown by solid bars). These results suggest that the more central events at RHIC are in fact consistent with hydrodynamic evolution. The models used here typically start with energy densities around 20 GeV/fm^3 evolving from an early time $\tau < 1$ fm, which is consistent with values extracted from the saturation approach.

The importance of v_2 as an experimental observable comes from the quantitative comparisons with theoretical predictions for observables relative to the reaction plane, which is defined as the axis where $dN/d\phi$ is at a maximum. Measurements of v_2 as a function of the transverse momentum [17] characterize the modulation of $dN/d\phi$ for particles of a given momentum relative to the reaction plane. As seen in Fig. 10, STAR has measured $v_2(p_T)$ for different particle species

and found good agreement with hydro calculations out to $p_T \sim 1$ GeV, where their particle identification stops. However, two notable disagreements with hydro exist. The linear rise of v_2 with p_T stops at $p_T \sim 2$ GeV and remains constant out to larger p_T [17]. Also, the pseudorapidity distribution of v_2 drops rapidly away from midrapidity, suggesting that the "boost-invariant" hydrodynamic behavior may only be found very near $y = 0$ [18].

6 Thermal Description of the Final Hadronic State

As the system expands and cools, it eventually hadronizes into the final state particles measured in the detectors. As these are the particles identified by most of the experiments, a large amount of data exists on the properties of this stage, only a subset of which will be shown in this section. The most pressing issue is whether the final state shows collective effects, which would be a signal of equilibration, as opposed to particle production simply proceeding via the available phase space.

The most basic property of the system, measured by all four RHIC experiments, is the gradual approach of all of the anti-particle/particle ratios towards unity [19], as shown in Fig. 11. The fact that $\overline{p}/p$ is less than unity directly indicates the presence of some fraction the primary baryons at mid-rapidity, an incredible fact considering the large initial baryon momentum. The kaons, while approaching one, also do not reach it at the top RHIC energy. These two ratios have been found to be highly correlated, suggesting that the produced hadrons are highly sensitive to the net baryon density. Still, RHIC is closer than ever before to creating the conditions found in the very early universe.

The relationship between these ratios, and many others, can be understood by means of "thermal models"[20], which assume the system to be in chemical and thermal equilibrium up to the time when the momentum transfers are low enough that the flavor composition of the system is frozen. If only the ratios of particle yields are used, then the available parameters are simply T (the temperature), μ_B (the baryon chemical potential) and γ_s, which parameterizes the deviation from full strangeness equilibration. A volume (V) is needed if absolute yields are to be characterized as well.

The application of these models to data from central collisions of heavy nuclei, as a function of $\sqrt{s}$, finds the simple result (shown in Fig. 2) that all of the data seem to lie on a single contour on the (T, μ_B) space. There are two interpretations of this behavior [20]. Cleymans *et al.* explain this as freezeout occurring when the energy per particle $\langle E \rangle / \langle N \rangle \sim 1$ GeV. Braun-Munzinger and Stachel suggest

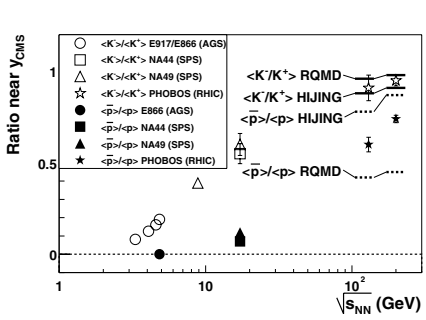

Figure 11: PHOBOS ratios of anti-particle to particle vs. $\sqrt{s}$

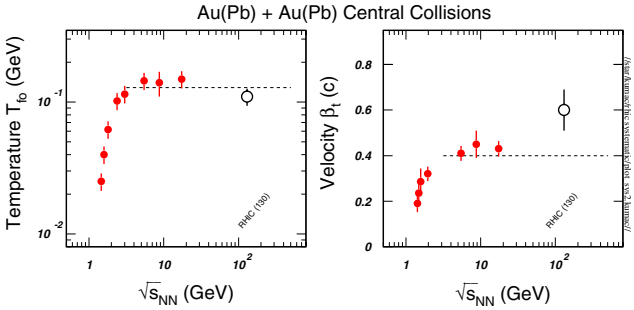

Figure 12: Thermal freezeout parameters shown as a function of $\sqrt{s}$.

that it occurs at a constant total baryon density of $n_B = .12/\text{fm}^3$. Both of these interpretations are consistent with the existing data.

It is interesting that thermal models have also been applied to pp, $\overline{p}p$ and e^+e^- data and find the similar result of $T \sim 170$ MeV (with $\mu_B = 0$) [21]. This suggests that the heavy ion data above CERN energies approaches similar freezeout state as that for elementary systems. This may be another indication of the onset of universal behavior as the role of the net baryon density becomes less significant. However, some important remain between heavy ions and the elementary systems.

One difference between nuclei and the more elementary systems is evident in the details of the momentum spectra. In elementary collisions (pp, e^+e^-), the spectra at low m_T show "m_T scaling" where the individual particle yields described by an exponential $\exp(-m_T/T)$ with same slope for all particle species. In heavy ions, the slope at low m_T increases with the particle mass in a way which can be fit by the form $T_{\text{eff}} = T_o + m\langle\beta\rangle^2$, where $\langle\beta\rangle$ is a collective "radial flow" velocity. The energy dependence of the fit parameters has been extracted by Kaneta and Xu [22] and is shown in Fig. 12. They observe a thermal freezeout temperature ($T_{th} = 140$ MeV) which is consistently lower than the chemical freezeout extracted from the particle ratios ($T_{ch} = 170$ MeV). They also find that $\langle\beta\rangle$ increases rapidly with $\sqrt{s}$ but appears to saturate above $\sqrt{s_{NN}} \sim 10$ GeV. These data strongly imply collective behavior among the final state hadrons.

Another important difference is seen in the total strangeness yield, which is "enhanced" by a factor of two in heavy ion collisions, as shown by the energy dependence of the "Wroblewski" factor ($\lambda_s = 2\langle\overline{s}s\rangle/(\langle\overline{u}u\rangle + \langle\overline{d}d\rangle)$) in Fig. 13. While strangeness enhancement has long been a canonical signal of QGP formation,

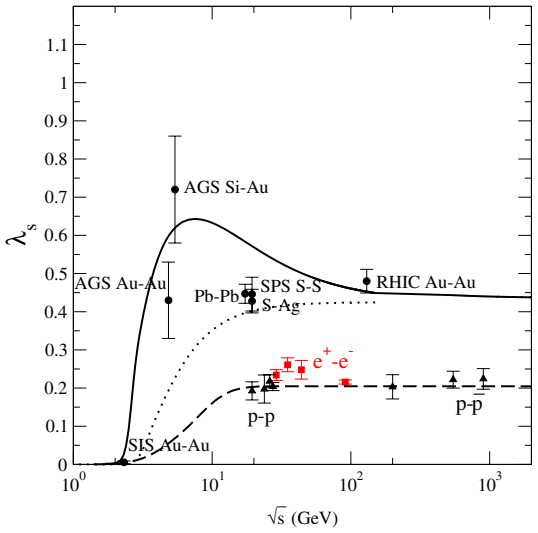

Figure 13: Energy and system dependence of the Wroblewski factor, which measures the ratio of strange to non-strange particle production.

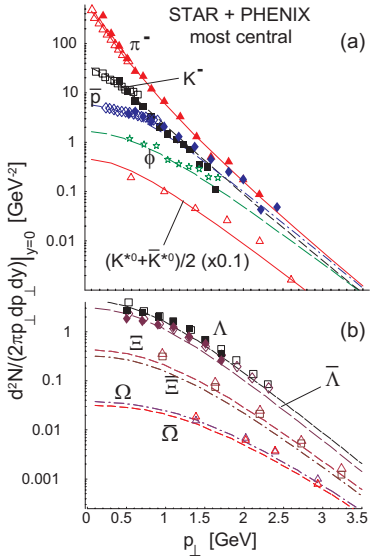

Figure 14: Single freeze-out time calculations for identified particle spectra by Broniowski and Florkowski.

there exists a simple interpretation of this effect in terms of the volume over which strangeness can equilibrate. In other words, the system produced in nuclear collisions no longer seems to be forced to obey *local* strangeness conservation [23]. However, a recent analysis by NA49 [24], characterizing the K^+/π^+ ratios as a function of centrality at CERN SPS energies, has shown that the effect may not be related precisely to the reaction volume. Instead, this ratio scales with the fraction of participants that have collided more than once, shifting the responsibility for what appears to be equilibration in the final state to some property of the initial collision geometry.

Both chemical and thermal freezeout is addressed in the model by Broniowski and Florkowski [25]. They assume that chemical and thermal freezeout occur at the *same* time. By fitting to the available π, K and p spectra from PHENIX and STAR, and incorporating transverse expansion, this model is able to describe all measured particle species, and was even successful in predicting particles like the $K^\star$ and Ω. The success in understanding the $K^\star$ yields is very interesting since it has a lifetime comparable to the lifetime of the system itself ($c\tau \sim 4$ fm). This suggests that there is little, if any, subsequent interactions of the $K^\star$ decay products, lending credibility to the assumption of the single freezeout time. This model is similar in concept to so-called "blast wave" fits to experimental data, which also

assumes that hadronization occurs on a thin space-time shell. The success of these two approaches suggests that the hadronization process is quite sudden.

7 Hard Probes of the Early Stages

Hard processes occur at early times ($\Delta t \sim \hbar/\Delta E$) and thus offer a means to probe the early stages of the collision. In principle, jet cross sections can still be calculated within a pQCD framework as they are for hadron-hadron interactions, by considering the structure of the nucleons in the colliding nuclei and assuming they interact via the standard pQCD matrix elements. Naively, one would expect that the rate of hard processes should scale with the number of binary collisions, since the timescale of hard processes is so short that incoming nucleons will be sensitive to all of the nucleons in its path. However, there is large body of theoretical work suggesting that high-energy partons should lose energy in a deconfined medium via color bremsstrahlung - a phenomenon called "jet quenching". Jets traversing a hadronic medium should suffer no induced radiation and thus be unmodified.

At RHIC energies, there are two impediments to directly measuring jets. First of all, the typical energy is not high enough to create well-collimated cones of particles. Secondly, a central event always creates a large background of soft particles which will obscure a jet signal within a typical jet cone. Thus, measurements of quenching focus primarily on the high-p_T part of the inclusive hadron spectrum, to look for modifications to the measured jet fragmentation functions.

First results on particle spectra at high p_T in heavy ion collisions were shown by the PHENIX and STAR collaborations only a few months after the end of the 130 GeV RHIC running in 2000 [26]. Both collaborations presented the modification of the inclusive hadron spectra (both of all charged particles and identified π^o's) in central Au+Au collisions by a ratio comparing it with spectra from $\overline{p}p$ collisions measured by the UA1 collaboration, interpolated to 130 GeV and then divided by the number of binary collisions.

$$R_{AA} = \frac{dN/dp_T(\mathrm{Au}+\mathrm{Au})}{N_{coll} \times dN/dp_T(\overline{p}p)} \tag{1}$$

The PHENIX results of R_{AA} vs. p_T for charged hadrons and neutral pions in 130 GeV Au+Au collisions are shown in Fig. 15. At low-p_T, the R_{AA} is 1/6, as expected for wounded nucleon scaling (since $N_{coll}/(N_{part}/2) \sim 6$ in central Au+Au). However, while R_{AA} increases with p_T, as might be expected for the gradual dominance of hard processes, at 2 GeV the rise stops, with R_{AA} saturating or decreasing, depending on the particle type, well below unity. STAR results

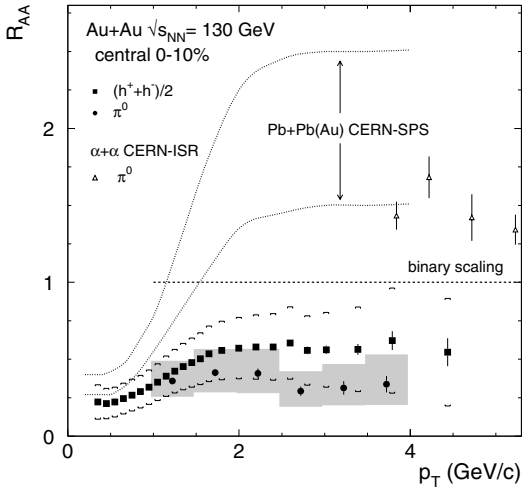

Figure 15: PHENIX results indicating suppression of high-p_T particle production in nuclear collisions.

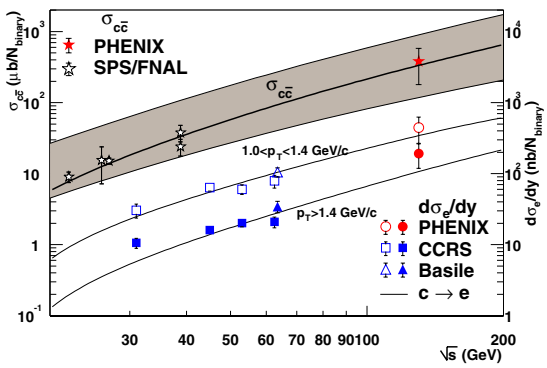

Figure 16: PHENIX results on the total charm cross section per binary collision, compared with lower energy pp data.

on R_{AA} show a marked decrease above 2 GeV. Preliminary results at 200 GeV from both experiments confirm this decrease and find that above 5-6 GeV, R_{AA} becomes approximately constant at $\approx 1/6$ out to 9 GeV (PHENIX all charged and π^o) and $\approx 1/3$-$1/2$ out to 11 GeV (STAR all charged). These results are in qualitative agreement with the jet quenching hypothesis and theoretical descriptions are rapidly becoming available.

While large energy loss effects were expected for the nearly-massless light quarks, heavy quarks are expected to radiate far less. This is because of the "dead-cone" effect, where radiation is suppressed at angles less than $\theta < m_q/E$, where m_q is the mass of the heavy quark, and E is its energy [27]. This expectation has been tested by PHENIX using measurements of single electrons and positrons in central 130 GeV Au+Au collisions. They observe a significant excess of electrons above the expected hadronic and photonic backgrounds and attribute it to the presence of open charm, thus extracting an open charm cross section per binary collision $\sigma_{\bar{c}c} = 380\mu b \pm 200(\text{sys}) \pm 60(\text{stat})$ [28]. This is consistent with an extrapolation of FNAL and ISR measurements using a PYTHIA calculation tuned to reproduce the lower energy results, as shown in Fig. 16.

Thus, there seems to be no violation of collision scaling in the charm sector, consistent with no energy loss, as expected from the dead-cone effect. However, it

must be kept in mind that this measurement has large systematic errors, which are being carefully addressed in the higher-statistics 200 GeV data. It should also be noted that the electrons have not been directly tagged as coming from charm decays, e.g. by measuring the characteristic decay length of the charm mesons. Future upgrades to the RHIC experiments seek to address this issue definitively, which is a crucial piece of information both for understanding jet quenching and as a baseline for J/Ψ suppression.

8 Ultra Peripheral Interactions

The colliding gold beams at RHIC have also opened up opportunities of studying the physics of coherent meson production. The highly compressed ions act as sources of very strong Coulomb fields as well as pomerons. Thus, at large impact parameter, one expects photon- photon or photon-pomeron interactions, as well as virtual photon exchange. Vector mesons can be produced coherently by a virtual photon, emitted by one nucleus, fluctuating into a quark-antiquark pair and scattering elastically off of the other nucleus, provided they satisfy the conditions $p_T < \pi\hbar/R_A$ (90 MeV) and $p_{||} < \pi\hbar\gamma/R_A$ (6 GeV) where γ is the lorentz boost of the nucleus (70 at RHIC 130 GeV). The ρ^o production cross section can be predicted using Glauber extrapolations of ρ^o photoproduction data to be 350 mb [29].

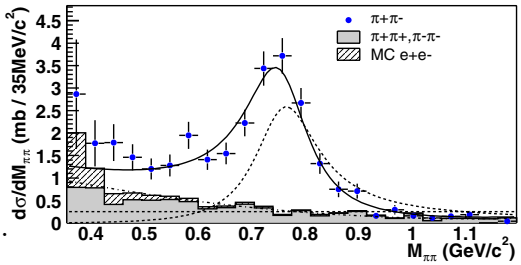

Figure 17: STAR results on coherent ρ^0 production in 130 GeV ultraperipheral Au+Au collisions.

Using a combination of special triggers and minimum-bias samples, STAR has extracted a strong coherent ρ^o peak both in collisions where the gold nuclei are intact, and where one or more neutrons is dissociated from each nucleus via coulomb excitation (shown in Fig. 17). They extract an exclusive ρ^o cross section of $410 \pm 190 \pm 100$ mb [30]. The agreement between these measurements and the Glauber predictions suggests that ρ^o production and Coulomb excitation are independent processes, and thus factorize. These measurements thus point to new opportunities in the physics of strong fields.

9 Summary of Results

With the new RHIC data, systematic data now exists for heavy ion collisions as a function of $\sqrt{s}$ over several orders of magnitude and as a function of impact

parameter. These data test the interplay between hard and soft processes in a large-volume system where nucleons are struck multiple times. The data is consistent with creating a deconfined state (jet quenching) that forms quickly (saturation models), expands rapidly (radial and elliptic flow) and freezes out suddenly (single freezeout and blast wave fits). There are also intriguing connections with particle production in elementary systems, which point to the role of the energy available for particle production on the features of the final state. Many in this field are optimistic that the careful understanding of this experimental data may lead to the theoretical breakthroughs that will connect these complex systems to the fundamental lattice predictions.

Acknowledgments

I would like to thank the organizers of Physics in Collision for inviting me to speak on behalf of the heavy ion community. I would also like to thank the RHIC experiment spokespeople, W. Busza, T. Hallman, F. Vidaebeck, and W. Zajc, for their input. Finally, special thanks to J. Nagle, C. Roland, and the PHOBOS collaboration for valuable suggestions and advice while preparing the talk and manuscript.

References

1. F. Karsch, Lect. Notes Phys. **583**, 209 (2002).
2. Proceedings of "Quark Matter 2002", forthcoming.
3. I. G. Bearden, arXiv:nucl-ex/0207006.
4. W. Busza and A. S. Goldhaber, Phys. Lett. B **139**, 235 (1984).
5. K. Adcox *et al.*, Phys. Rev. Lett. **87**, 052301 (2001).
6. B. B. Back *et al.*, Phys. Rev. Lett. **88**, 022302 (2002). B. B. Back *et al.* ,Phys. Rev. C **65**, 061901 (2002).
7. D. Kharzeev and M. Nardi, Phys. Lett. B **507**, 121 (2001).
8. E. Iancu, A. Leonidov and L. McLerran, arXiv:hep-ph/0202270.
9. D. Kharzeev and E. Levin, Phys. Lett. B **523**, 79 (2001).
10. M. Basile *et al.*, Phys. Lett. B **92**, 367 (1980). M. Basile *et al.*, Phys. Lett. B **95**, 311 (1980).

11. B. B. Back *et al.*, forthcoming. P. Steinberg, in Ref. [2].

12. A. H. Mueller, Nucl. Phys. B **213**, 85 (1983).

13. J. E. Elias *et al.* Phys. Rev. Lett. **41**, 285 (1978).

14. S. V. Afanasiev *et al.*, arXiv:nucl-ex/0205002 (2002).

15. R. Devenish, these proceedings.

16. P. F. Kolb, J. Sollfrank and U. W. Heinz, Phys. Lett. B **459**, 667 (1999). P. F. Kolb, P. Huovinen, U. W. Heinz and H. Heiselberg, Phys. Lett. B **500**, 232 (2001).

17. K. H. Ackermann *et al.*, Phys. Rev. Lett. **86**, 402 (2001). C. Adler *et al.*, Phys. Rev. Lett. **87**, 182301 (2001).

18. B. B. Back *et al.*, arXiv:nucl-ex/0205021.

19. B. B. Back *et al.*, arXiv:nucl-ex/0206012.

20. J. Cleymans and K. Redlich, Phys. Rev. Lett. **81**, 5284 (1998). P. Braun-Munzinger and J. Stachel, J. Phys. G **28**, 1971 (2002).

21. F. Becattini, Z. Phys. C **69**, 485 (1996).

22. M. Kaneta and N. Xu, J. Phys. G **27**, 589 (2001).

23. J. Cleymans, arXiv:hep-ph/0201142.

24. C. Hohne, in Ref. [2].

25. W. Broniowski and W. Florkowski, Phys. Rev. C **65**, 064905 (2002).

26. K. Adcox *et al.*, Phys. Rev. Lett. **88**, 022301 (2002). C. Adler *et al.*, arXiv:nucl-ex/0206011.

27. Y. L. Dokshitzer and D. E. Kharzeev, Phys. Lett. B **519**, 199 (2001).

28. K. Adcox *et al.*, Phys. Rev. Lett. **88**, 192303 (2002).

29. S. Klein and J. Nystrand, Phys. Rev. C **60**, 014903 (1999).

30. C. Adler *et al.*, arXiv:nucl-ex/0206004.